Precambrian Research 347 (2020) 105835

Contents lists available at ScienceDirect

Precambrian Research

journal homepage: www.elsevier.com/locate/precamres

Mesoproterozoic paleo-redox changes during 1500–1400 Ma in the Yanshan Basin, North China

Xiaoyan Chen[a], Menghan Li[a], Erik A. Sperling[b], Tonggang Zhang[c], Keqing Zong[d], Yongsheng Liu[d], Yanan Shen[a,*]

[a] School of Earth and Space Sciences, University of Science and Technology of China, Hefei 230026, China
[b] Department of Geological Sciences, Stanford University, Stanford, CA 94305, USA
[c] College of Geosciences, China University of Petroleum, Beijing 102249, China
[d] State Key Laboratory of Geological Processes and Mineral Resources, Faculty of Earth Sciences, China University of Geosciences, Wuhan 430074, China

ARTICLE INFO

Keywords:
Mesoproterozoic
Fe species
Redox sensitive metals
Redox conditions

ABSTRACT

The Mesoproterozoic (1600–1000 million years ago, Ma) is thought to have experienced important changes in ocean chemistry and eukaryote evolution. Our understanding of global redox conditions remains in its infancy, and redox data derived from the Mesoproterozoic thus far indicate heterogeneity and complexity in the realm of ocean redox, which hampers our understanding of the potential significance of variations in ocean redox on eukaryote evolution. In this study, we report analyses of Fe species and redox-sensitive trace metals of U and Mo from the Jixian Group, including the Wumishan, Hongshuizhuang and Tieling formations, as well as the Xiamaling Formation, in the Yanshan Basin in North China. The Fe speciation data from the Wumishan, Hongshuizhuang, and Tieling formations first reported in this study help bridge the global data gap of Fe species data during 1500–1400 Ma. Our data suggest likely oxic bottom water conditions for the Wumishan Formation and ferruginous bottom water conditions for the Tieling Formation. The Fe species data can distinguish ferruginous conditions for the upper Hongshuizhuang from sulfidic depositional conditions for the lower-middle Hongshuizhuang Formation. Based on Fe species and trace metal data, redox conditions likely varied from anoxic conditions with transient euxinia in the lower-middle Xiamaling Formation to oxic conditions in the upper Xiamaling Formation. The new Fe speciation data from the Yanshan Basin, when combined with previously published data, show a surprisingly high proportion of middle Proterozoic samples with very low highly reactive to total iron ratios. This suggests either a relatively large extent of oxic seafloor, or non-uniformitarian iron cycling. Resolving this discrepancy will be key to understanding the extent of suitable habitats for complex eukaryotes.

1. Introduction

The oxygenation of the Earth's atmosphere and oceans is one of the most important issues in studying Precambrian biogeochemical cycles. The Mesoproterozoic era (1600–1000 Ma) witnessed the significant changes of the ocean chemistry as well as the onset and diversification of multicellular eukaryotes (Anbar and Knoll, 2002; Kah and Bartley, 2011; Butterfield, 2015; Cohen and Macdonald, 2015). It also records the greatest range in stromatolite forms, basin-wide sulfate evaporites, and a full range of distinct carbonate facies from sea floor cements to molar-tooth structure (Kah and Knoll, 1996; Grotzinger and Knoll, 1999; Kah et al., 2001, 2004; Shields, 2002; Pollock et al., 2006) as well as significant changes in the biogeochemical cycles of carbon, sulfur and oxygen (Buick et al., 1995; Kah et al., 1999; Bartley and Kah, 2004; Parnell et al., 2010; Reinhard et al., 2013; Crockford et al., 2018, 2019).

Unlike the generally accepted hypothesis of an anoxic Archean atmosphere and ocean with local oxygen oases (Farquhar et al., 2000; Anbar et al., 2007), and a well-oxygenated Phanerozoic ocean with local and episodic anoxia, the redox environment during the middle Proterozoic has been extensively examined to better understand the evolution of Proterozoic atmospheric O_2 and its potential link to delayed eukaryotic diversification. Numerous geochemical and modeling studies have been conducted to reconstruct paleo-redox changes in marine basins worldwide (Canfield, 1998; Shen et al., 2002, 2003; Arnold et al., 2004; Poulton et al., 2004; Scott et al., 2008; Kendall et al., 2011; Gilleaudeau and Kah, 2013, 2015; Planavsky et al., 2011,

* Corresponding author at: School of Earth and Space Sciences, University of Science and Technology of China, Hefei 230026, China.
E-mail address: yashen@ustc.edu.cn (Y. Shen).

https://doi.org/10.1016/j.precamres.2020.105835
Received 24 January 2020; Received in revised form 8 June 2020; Accepted 22 June 2020
Available online 26 June 2020
0301-9268/

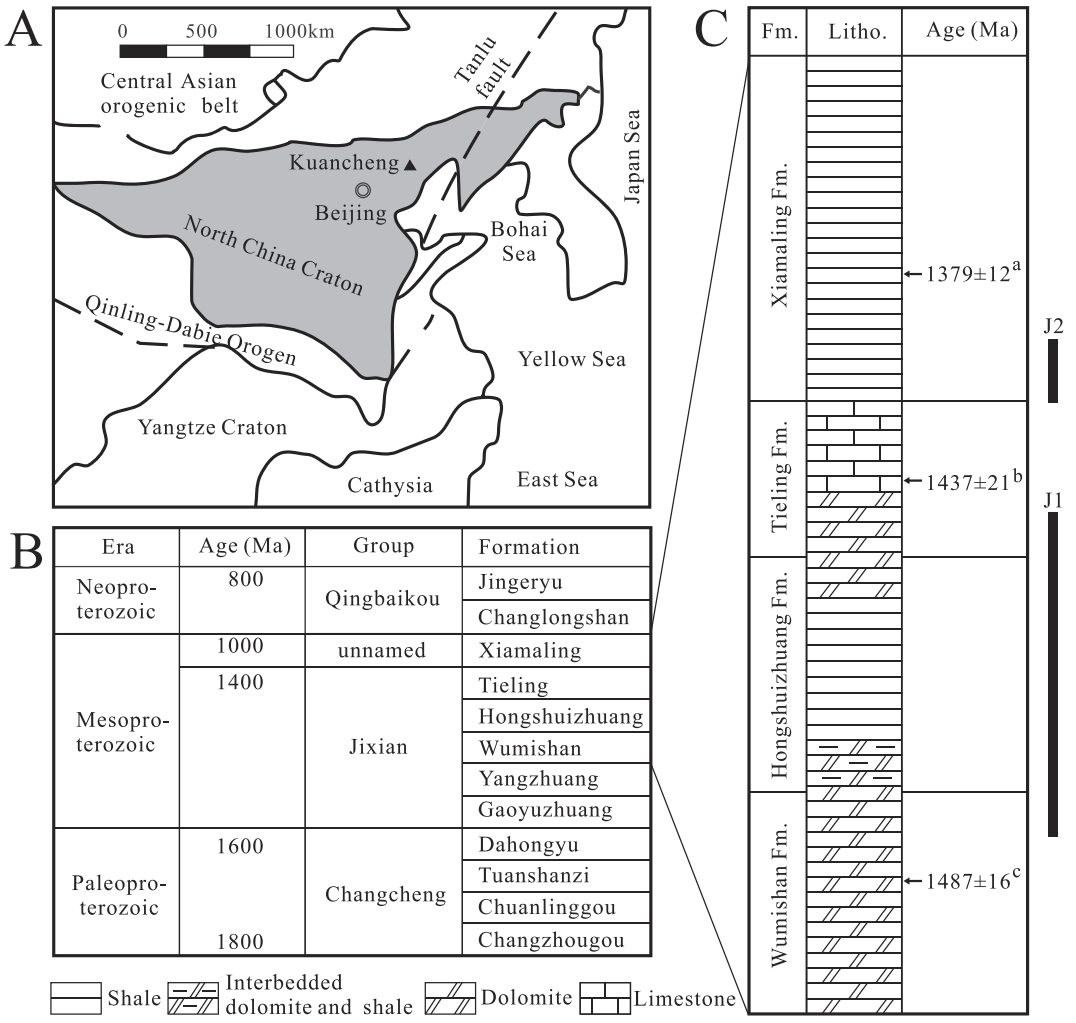

Fig. 1. (A). Map of the Yanshan Basin, North China Craton (modified from Luo et al., 2013). The triangle indicates the location of drill cores J1 (40°34.649 N, 118°21.219E) and J2 (40°34.902 N, 118°21.515E). (B). Stratigraphic succession of the Proterozoic in the Yanshan Basin. The black bars represent drill cores J1 and J2. (C). Stratigraphic sequence of drill cores J1 and J2 and the zircon U-Pb age constraints for each formation. a = Su et al. (2008); b = Su et al. (2010); c = Li et al. (2014).

2014; Luo et al., 2015; Slotznick et al., 2018; Zheng et al., 2018; Gilleaudeau et al., 2016, 2019). Using various proxies, these studies have provided evidence for either long-term or episodic anoxic or sulfidic oceans during the middle Proterozoic, rather than for a fully oxic ocean. However, the spatial structure of redox conditions in the Mesoproterozoic oceans remains controversial. A growing body of evidence indicates more complex changes in middle Proterozoic ocean chemistry in space and time than was previously thought and have shown episodic oxygenations and redox heterogeneity of subsurface water masses (Kah et al., 1999, 2004; Poulton et al., 2010; Partin et al., 2013; Sperling et al., 2014; Gilleaudeau and Kah, 2015; Zhang et al., 2016a; Zhang et al., 2018; Yang et al., 2017; Planavsky et al., 2018; Diamond et al., 2018; Gilleaudeau et al., 2019). The controversy may arise from the different marine basins that have been studied, the different proxies that have been applied, or different interpretations of similar geochemical data.

One of the best successions worldwide for addressing questions about the redox structure of Mesoproterozoic oceans may be represented by the broadly continuous sedimentary environments of the Yanshan Basin in North China (Fig. 1). Indeed, the data from the Yanshan Basin have greatly improved our understanding of Proterozoic ocean chemistry changes. The $\delta^{34}S$ data of carbonate-associated sulfate (CAS) suggest the development of euxinic bottom-water conditions as well as a modest increase in the oceanic sulfate concentration between ~1560 Ma and ~1483 Ma in the Yanshan Basin (Guo et al., 2013, 2015; Luo et al., 2014, 2015). The Fe species data, cerium anomaly, and I/(Ca + Mg) ratios from the Gaoyuzhuang Formation in the Yanshan Basin suggest oxygenation at ~ 1560 Ma which was thought to have facilitated the evolution of complex eukaryotes (Zhang et al., 2018; Shang et al., 2019). Geochemical data measured from the younger successions in the Yanshan Basin have also improved our knowledge about the evolution of the Proterozoic ocean and atmosphere and possible links between environmental changes and the evolution of early life. Biomarkers, Fe speciation, and trace metal redox proxies from the Xiamaling Formation (~1400 Ma) suggest an atmospheric oxygen level of ≥3.8% PAL, which may be sufficient for animal respiration, although deeper waters may still have remained anoxic (Zhang et al., 2016a, 2017, 2019; Wang et al., 2017). However, this hypothesis has been challenged and extensively debated (Planavsky et al., 2016; Zhang et al., 2016b). The contrasting views between Planavsky et al. (2016) and Zhang et al. (2016b) are essentially about the interpretation of low V/Al and Fe_{HR}/Fe_T ratios as well as primary nature of biomarker data reported from the Xiamaling Formation by Zhang et al. (2016a). The similarly low Fe_{HR}/Fe_T ratios (< 0.38) measured from the Xiamaling Formation reported by Zhang et al. (2016a) and Diamond et al. (2018) have yielded contrasting interpretations. Zhang et al. (2016a) argued that the low Fe_{HR}/Fe_T (< 0.38) ratios demonstrate bottom water oxygenation near the seafloor during the deposition of three of the four

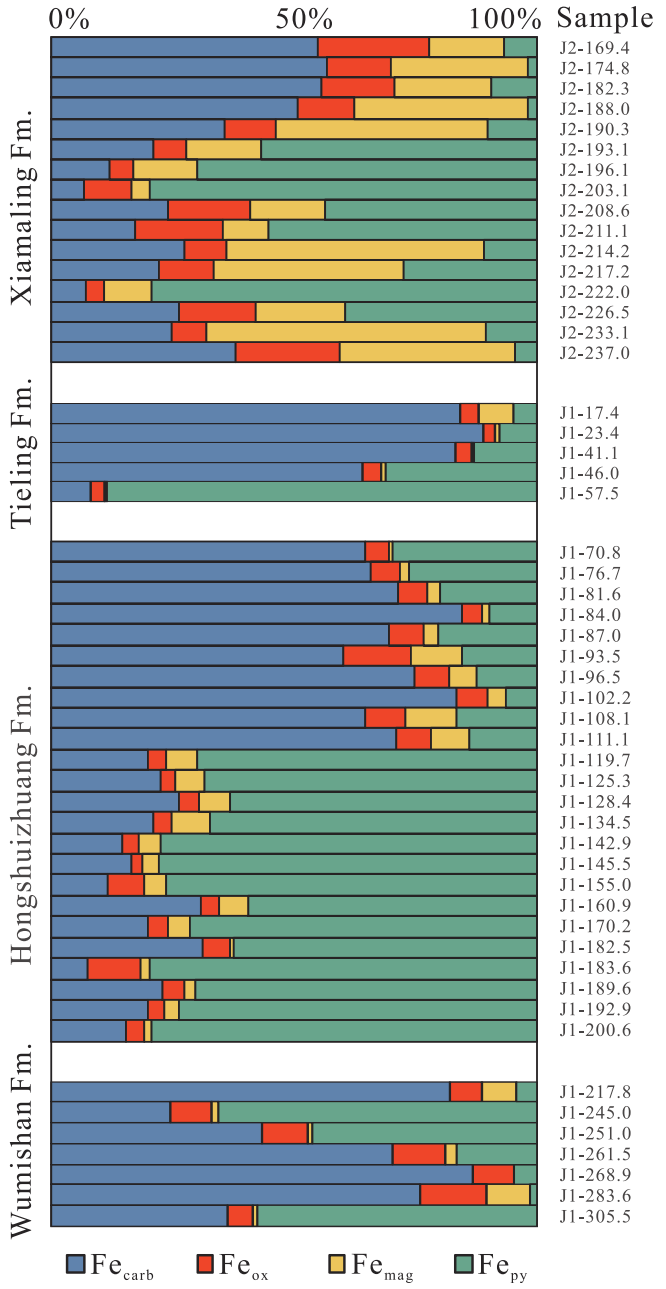

Fig. 2. Percentages of each species of Fe_{HR} for each sample showing the proportion of Fe_{carb}, Fe_{py}, Fe_{ox}, and Fe_{mag} in Fe_{HR}.

units of the Xiamaling Formation (see also Wang et al., 2017; Zhang et al., 2017, 2019). By contrast, Diamond et al. (2018) argued that the low Fe_{HR}/Fe_T ratios may have resulted from the lack of sufficient Fe_{HR} in the basin, which was restricted at the time the Xiamaling Formation was deposited.

Given the importance of the Yanshan Basin as a source of evidence for the redox structure of the Mesoproterozoic oceans, we analyzed Fe speciation and trace metal (Mo, U) concentrations from drill core samples of the Jixian Group, including the Wumishan, Hongshuizhuang and Tieling formations, as well as the Xiamaling Formation, to constrain the paleo-redox changes in the Yanshan Basin (Fig. 1). To our knowledge, no previous study has reported Fe speciation data from the Wumishan, Hongshuizhuang and Tieling formations in the Yanshan Basin. Fe speciation data are particularly valuable for distinguishing ferruginous conditions from sulfidic depositional conditions (Raiswell and Canfield, 1998; Raiswell et al., 2018; Sperling et al., 2015). New Fe speciation and trace metal data from the Yanshan Basin therefore provides a new insight into changes in Mesoproterozoic ocean chemistry and their possible link to the early evolution of complex eukaryotes.

2. Geological setting

The Yanshan Basin in the North China Craton represents low-latitude deposition in an intracratonic rift, which was subsequently transformed to a passive margin after the breakup of the Columbia supercontinent (Zhao et al., 2002; Lu et al., 2008) (Fig. 1). The unmetamorphosed sedimentary sequences are well preserved, relatively well dated to the early Mesoproterozoic, and appears generally continuous with no large unconformities relative to the span studied. Strata of the Yanshan Basin unconformably overlie Archean and late Paleoproterozoic metamorphic basement (Lu et al., 2008). The sedimentary succession is commonly divided into four groups (Fig. 1): the Changcheng Group (1800–1600 Ma), Jixian Group (1600–1400 Ma), an unnamed group (1400–1000 Ma), and the Qingbaikou Group (1000–800 Ma) (Qiao et al., 2007). The Jixian Group, consisting of five formations (the Gaoyuzhuang, Yangzhuang, Wumishan, Hongshuizhuang and Tieling formations), is dominated by finely-laminated to stromatolitic dolomite and siliciclastic sediment. The Xiamaling Formation, assigned to the unnamed group, is mainly composed of organic-rich shale (Qiao et al., 2007).

Our samples were collected from two drill cores from the Wumishan, Hongshuizhuang, Tieling and Xiamaling formations (Fig. 1). Drill core Jiqian1 (J1) (40°34.649 N, 118°21.219E) contains the upper part of the Wumishan Formation, the Hongshuizhuang Formation and the lower part of the Tieling Formation, in ascending order (Fig. 1). The Wumishan Formation is characterized by dolomite and stromatolites with thinly-bedded microbial dolomite. Rhythmic magnesium-rich carbonate in the Wumishan Formation have been interpreted to have been deposited in a peritidal or epicontinental sea (Zhao, 1988). Ages of 1483 ± 13 Ma and 1487 ± 16 Ma for the bentonite beds from the Wumishan Formation were obtained by SHRIMP zircon U-Pb dating (Li et al., 2014).

The lower Hongshuizhuang Formation, conformably overlying the Wumishan Formation, consists of finely laminated shale and dolomite with rhythmic stratification. The middle Hongshuizhuang Formation is composed of black shale with pyrite and glaucony, followed by silty dolomite with micritic dolomite in the upper section. The Hongshuizhuang Formation was suggested to have been deposited in a subtidal to shallow sea environment, with the middle section representing the deepest water depth (Luo et al., 2013).

The uppermost part of the Jixian Group is the Tieling Formation (Fig. 1). The lower part of the formation consists mainly of stromatolitic dolomite interbedded with thin Mn-rich and K-rich shale, which is interpreted as representing fluctuating water depths from deep subtidal to intertidal (Mei et al., 2008). The upper part of the formation consists of limestone, which was suggested to have been deposited in shallow subtidal to intertidal environments (Mei et al., 2008). A U-Pb zircon age of 1437 ± 21 Ma was obtained for a K-bentonite bed in the Tieling Formation (Su et al., 2010).

Samples of the Xiamaling Formation were collected from drill core Jiqian2 (J2) (40°34.902 N, 118°21.515E). The Xiamaling Formation is characterized by stromatolitic carbonate and shale with parallel bedding and cross bedding, suggesting shallow depositional environments (Wang and Li, 1993). The Xiamaling Formation in the Xiahuayuan region was divided into six units, and our samples are from the lower Xiamaling Formation from drill core J2, which may be correlative with Unit 6 in Wang et al. (2017). A series of U-Pb ages (Fig. 2) of ~ 1380 Ma for zircons from the Xiamaling Formation have provided age constraints (e.g., Su et al., 2008).

3. Redox proxies and analytical methods

3.1. Fe speciation

Iron speciation is widely used as a proxy for reconstructing the redox conditions of the ancient local water column. The proxy is based on the ratio of highly reactive iron (Fe_{HR}) to total iron (Fe_T), which distinguishes anoxic conditions from oxic conditions. Fe_T refers to the total iron content of a sample, and highly reactive iron (Fe_{HR}) refers to iron that is sufficiently reactive to form pyrite (Raiswell and Canfield, 1998), including carbonate-associated iron (Fe_{carb}), ferric (oxyhydr) oxides (Fe_{ox}), magnetite iron (Fe_{mag}) and iron sulfide minerals (Fe_{py}) (Poulton and Canfield, 2005). Calibration of iron speciation based on modern and ancient marine sediments suggests that $Fe_{HR}/Fe_T < 0.38$ indicates oxic bottom water, while $Fe_{HR}/Fe_T > 0.38$ suggests anoxic conditions (Raiswell and Canfield, 1998; Raiswell et al., 2018). Sediments deposited under anoxic conditions may be enriched in Fe_{HR} from the upwelling of Fe (II)-rich anoxic water, or to the export of remobilized Fe from the oxic shelf (Raiswell and Canfield, 1998). Equivocal conditions are inferred when the ratios are between 0.22 and 0.38, because with rapid sedimentation rates or turbiditic conditions, Fe_{HR} enrichment could be masked (Raiswell and Canfield, 1998; Raiswell et al., 2018). Carbonate-rich samples with $Fe_T < 0.5\%$ may yield erroneously high Fe_{HR}/Fe_T ratios, which would suggest anoxic conditions if interpreted in the standard framework, in contrast to the evident oxic depositional conditions (Clarkson et al., 2014; Raiswell et al., 2018).

The Fe speciation proxy can also distinguish euxinic conditions from ferruginous conditions, based on the ratios of Fe_{py}/Fe_{HR}. A euxinic water column may be indicated when $Fe_{py}/Fe_{HR} > 0.7$ (Raiswell et al., 2018). The Fe_{py}/Fe_{HR} reaches 0.8 based on modern samples for which Fe_{mag} and Fe_{carb} were not measured. When the measurements of Fe_{mag} and Fe_{carb} are included, the threshold changes to 0.7, which may be more appropriate (Raiswell et al., 2018). However, these thresholds should be interpreted together with the Fe_{HR}/Fe_T ratio, as well as with other geochemical and geological data (Raiswell et al., 2018); the sum of the data is more important than strict baseline values.

3.2. Redox-sensitive trace metals

Trace metals such as Mo and U can be used as redox proxies for ancient sediments (Tribovillard et al., 2006). In oxic water, Mo exists as the unreactive molybdate oxyanion (MoO_4^{2-}), which is soluble in the water column and results in low enrichment in oxic marine sediments (Zheng et al., 2000). With the reaction of free sulfide, the molybdate oxyanion is converted to thiomolybdates which are readily adsorbed to the particle surfaces of Mn and Fe oxyhydroxides as well as organic matter, resulting in strong Mo enrichment in sediments deposited under euxinic conditions (Helz et al., 1996).

In an oxic water column, U exists as soluble U (VI) in the form of uranyl carbonate complexes ($UO_2(CO_3)_3^{4-}$) (Calvert and Pedersen, 1993; Tribovillard et al., 2006). As dissolved U (VI) cannot be scavenged by particles (Anderson et al., 1989), U (VI) enrichment is limited in oxic sediments (Morford et al., 2009). Under anoxic conditions, U (VI) is reduced to U (IV), and precipitates as insoluble UO_2, U_3O_7 and U_3O_8, resulting in U enrichment in sediments (McManus et al., 2005).

Observations of Mo and U enrichment in modern anoxic or sulfidic sediments have been applied to constrain anoxic depositional conditions in geological history (e.g., Tribovillard et al., 2006). However, low dissolved reservoirs of U and Mo were demonstrated in the Mesoproterozoic oceans compared to modern marine environments (Scott et al., 2008; Partin et al., 2013). Therefore, less enrichment of U and Mo in anoxic and sulfidic Mesoproterozoic sediments, relative to modern marine sediments, may be expected.

3.3. Iron speciation analyses

The drill core samples were crushed into small pieces and milled to < 200 mesh size using a Vibratory Disc Mill RS 200. Sequential extraction described in Poulton and Canfield (2005) was used to extract three pools of Fe_{HR} (Fe_{carb}, Fe_{ox} and Fe_{mag}) and all Fe species were measured at Historical Geobiology Laboratory, Stanford University. Approximately 100–150 mg of powdered rock was treated with 1 M sodium acetate, adjusted to pH 4.5 with acetic acid, for 48 h at 50 °C on a shaking table in order to extract Fe_{carb}. Fe_{ox} was extracted from the sample residue with 50 g/L of sodium dithionite solution buffered with acetic acid and 0.2 M sodium citrate, adjusted to pH 4.8, for 2 h at room temperature. Fe_{mag} was then extracted by treatment with a solution of 0.2 M ammonium oxalate and 0.17 M oxalic acid buffered with ammonium hydroxide adjusted to pH 3.2 for 6 h at room temperature. Fe_{mag} values measured using the oxalate extraction may include not only magnetite, but also other Fe-rich clay minerals such as berthierine and chamosite (Slotznick et al., 2018, 2020). The iron content of each extraction solution was measured with a Thermo Genesys 10S UV–Vis Spectrophotometer using HEPES-ferrozine-HCl solution, following Stookey (1970), with color development allowed to proceed overnight. The precision of sequentially extracted Fe is better than 5% for samples with appreciable iron (Sperling et al., 2015).

Powdered samples were then subjected to chromium reduction (Canfield et al., 1986) in order to convert pyrite sulfur to Ag_2S. Fe_{py} was determined stoichiometrically based on the pyrite sulfur content, assuming that the iron sulfide is present as FeS_2. However, if acid-volatile sulfides (AVS) are present, the content of Fe_{py} would be incorrect, as other metal sulfides (e.g., Cu, Ni, Zn) and iron monosulfides are also extracted by the chromium reduction method. Therefore, we tested four samples (J1-119.7, J1-125.3, J1-145.5 and J2-203.1) with high Fe_{py} contents for the presence of AVS using the 6 N HCl method described by (Rice et al., 1993). In AVS extractions, two samples (J1-145.5 and J2-203.1) showed no evidence for phases extractable in 6 N HCl. Two samples (J1-119.7 and J1-125.3) revealed small quantities of AVS. Assuming that all of the monosulfide we extracted was incorporated with Fe, the maximum calculated Fe content is 0.04%; however, with high pyrite contents, the AVS content has little effect on Fe_{py}.

3.4. Trace and major element analyses

A multiple acid (HNO_3-HF) digestion method was used to extract trace metal elements and Fe_T. Samples were chemically prepared following protocols in Liu et al. (2008). Specifically, powdered samples of ~50 mg were first digested in 1.5 ml HNO_3 and 1.5 ml HF in Teflon vessels at 190 °C for over 48 h. The liquid samples were then evaporated at 140 °C and the dried samples subsequently dissolved in 1 ml HNO_3 and again evaporated to dryness. The dried samples were dissolved in 3 ml of 30% HNO_3, sealed and heated at 119 °C for 12 h. The liquid samples were diluted with 2% HNO_3 in 50 ml constant volume bottles and analyzed with an Inductively Coupled Plasma Mass Spectrometer (ICP-MS) to obtain the trace metal and major element contents; the analyses were conducted at the State Key Laboratory of Geological Processes and Mineral Resources, China University of Geosciences, Wuhan.

Enrichment factors (EF) were calculated as:

$$X_{EF} = (X/Al)_{sample}/(X/Al)_{PAAS},$$

where X and Al are the weight percent of element X (X = Mo, U) and Al of samples and post-Archean average shale (PAAS), respectively (Taylor and McLennan, 1985).

Table 1
Fe species and trace metal (Mo, U) concentrations of the J1 and J2 drill core samples from the Yanshan Basin.

Formation	Depth (m)	Lithology	Fe_{carb} (%)	Fe_{ox} (%)	Fe_{mag} (%)	Fe_{py} (%)	Fe_{HR} (%)	Fe_T (%)	Fe_{HR}/Fe_T	Fe_{py}/Fe_{HR}	Mo (ppm)	U (ppm)	Al (%)	Mo_{EF}	U_{EF}
Xiamaling Fm (J2)	169.4	Shale	0.07	0.03	0.02	0.01	0.13	2.99	0.04	0.07	4.25	5.44	7.75	5.48	2.26
Xiamaling Fm (J2)	174.8	Shale	0.25	0.06	0.12	0.01	0.44	4.52	0.10	0.02	0.27	2.13	7.02	0.38	0.98
Xiamaling Fm (J2)	182.3	Shale	0.24	0.07	0.09	0.04	0.44	4.36	0.10	0.10	0.19	1.06	4.07	0.46	0.84
Xiamaling Fm (J2)	188.0	Shale	0.17	0.04	0.12	0.01	0.33	5.11	0.07	0.02	0.14	1.77	6.99	0.20	0.82
Xiamaling Fm (J2)	190.3	Shale	0.19	0.06	0.23	0.05	0.53	5.15	0.10	0.10	0.26	1.72	7.90	0.33	0.70
Xiamaling Fm (J2)	193.1	Shale	0.18	0.06	0.13	0.48	0.85	3.43	0.25	0.57	0.47	2.61	6.90	0.69	1.22
Xiamaling Fm (J2)	196.1	Shale	0.11	0.04	0.13	0.67	0.96	4.00	0.24	0.70	0.45	3.28	10.89	0.42	0.97
Xiamaling Fm (J2)	203.1	Shale	0.14	0.20	0.08	1.68	2.10	4.50	0.47	0.80	0.68	3.42	10.75	0.63	1.03
Xiamaling Fm (J2)	208.6	Shale	0.05	0.03	0.03	0.09	0.20	2.18	0.09	0.44	0.50	3.98	11.42	0.43	1.12
Xiamaling Fm (J2)	211.1	Shale	0.20	0.20	0.11	0.63	1.13	4.91	0.23	0.55	1.14	3.16	10.69	1.07	0.95
Xiamaling Fm (J2)	214.2	Shale	0.34	0.11	0.66	0.14	1.25	12.93	0.10	0.11	0.64	3.52	9.69	0.66	1.17
Xiamaling Fm (J2)	217.2	Shale	0.08	0.04	0.15	0.10	0.38	2.54	0.15	0.28	0.69	4.85		–	–
Xiamaling Fm (J2)	222.0	Shale	0.08	0.04	0.12	0.94	1.19	2.70	0.44	0.79	0.74	4.45	11.23	0.66	1.28
Xiamaling Fm (J2)	226.5	Shale	0.06	0.04	0.04	0.09	0.23	2.03	0.11	0.39	0.92	4.17	10.58	0.87	1.27
Xiamaling Fm (J2)	233.1	Shale	0.39	0.11	0.91	0.17	1.58	14.28	0.11	0.11	1.67	4.64	10.62	1.57	1.41
Xiamaling Fm (J2)	237.0	Shale	0.48	0.27	0.45	0.06	1.26	5.84	0.22	0.04	1.43	4.71	10.84	1.32	1.40
Tieling Fm.(J1)	17.4	Dolomite	1.10	0.05	0.09	0.06	1.31	1.68	0.78	0.05	0.16	0.63	1.46	1.12	1.39
Tieling Fm.(J1)	23.4	Dolomite	1.23	0.03	0.02	0.10	1.38	1.58	0.87	0.07	0.17	0.64	0.72	2.34	2.88
Tieling Fm.(J1)	41.1	Dolomite	0.39	0.02	0.00	0.06	0.46	0.61	0.76	0.13	0.09	0.62	0.75	1.15	2.67
Tieling Fm.(J1)	46.0	Dolomite	0.34	0.02	0.00	0.17	0.53	0.65	0.82	0.31	0.65	0.74	0.97	6.67	2.46
Tieling Fm.(J1)	57.5	Dolomite	0.07	0.03	0.00	0.79	0.90	0.96	0.93	0.88	0.74	0.70	1.51	4.88	1.50
Hongshuizhuang Fm.(J1)	70.8	Dolomite	0.36	0.03	0.00	0.17	0.56	0.94	0.59	0.30	0.29	1.87	3.17	0.93	1.90
Hongshuizhuang Fm.(J1)	76.7	Dolomite	0.27	0.02	0.01	0.11	0.41	1.11	0.37	0.26	0.92	3.47	5.34	1.73	2.10
Hongshuizhuang Fm.(J1)	81.6	Dolomite	0.42	0.04	0.01	0.12	0.59	1.43	0.41	0.20	0.17	1.89	4.17	0.40	1.46
Hongshuizhuang Fm.(J1)	84.0	Dolomite	0.50	0.02	0.01	0.06	0.59	1.03	0.57	0.09	0.24	1.95	2.54	0.95	2.47
Hongshuizhuang Fm.(J1)	87.0	Dolomite	0.46	0.05	0.02	0.13	0.66	1.71	0.38	0.20	0.11	2.01	4.42	0.26	1.47
Hongshuizhuang Fm.(J1)	93.5	Shale	0.26	0.06	0.05	0.07	0.43	2.00	0.21	0.15	0.20	2.61	6.64	0.30	1.27
Hongshuizhuang Fm.(J1)	96.5	Shale	0.59	0.06	0.04	0.10	0.79	1.98	0.40	0.12	0.18	1.59	4.32	0.42	1.19
Hongshuizhuang Fm.(J1)	102.2	Shale	0.69	0.05	0.03	0.05	0.82	1.90	0.43	0.06	0.15	1.74	4.21	0.35	1.34
Hongshuizhuang Fm.(J1)	108.1	Shale	0.49	0.06	0.08	0.12	0.76	1.91	0.40	0.16	0.31	2.27	3.57	0.88	2.05
Hongshuizhuang Fm.(J1)	111.1	Shale	0.55	0.06	0.06	0.11	0.77	1.69	0.46	0.14	0.23	2.16	5.63	0.41	1.24
Hongshuizhuang Fm.(J1)	119.7	Shale	0.31	0.06	0.10	1.08	1.54	2.99	0.52	0.70	34.6	8.28	6.45	53.66	4.14
Hongshuizhuang Fm.(J1)	125.3	Shale	0.41	0.06	0.10	1.25	1.83	2.87	0.64	0.69	52.3	10.1	6.14	85.17	5.32
Hongshuizhuang Fm.(J1)	128.4	Shale	0.45	0.06	0.11	1.07	1.70	2.62	0.65	0.63	39.7	8.97	6.41	61.87	4.52
Hongshuizhuang Fm.(J1)	134.5	Shale	0.27	0.04	0.10	0.85	1.27	2.50	0.51	0.67	63.3	10.4	6.14	103.13	5.48
Hongshuizhuang Fm.(J1)	142.9	Shale	0.24	0.06	0.07	1.26	1.62	3.06	0.53	0.77	56.9	10.7	5.79	98.26	5.95
Hongshuizhuang Fm.(J1)	145.5	Shale	0.32	0.05	0.07	1.53	1.96	3.01	0.65	0.78	50.0	10.4	4.61	108.50	7.29
Hongshuizhuang Fm.(J1)	155.0	Shale	0.15	0.09	0.06	0.97	1.26	2.14	0.59	0.76	5.46	4.84	6.49	8.41	2.40
Hongshuizhuang Fm.(J1)	160.9	Shale	0.22	0.03	0.04	0.42	0.71	1.77	0.40	0.59	23.6	7.44	5.91	39.99	4.07
Hongshuizhuang Fm.(J1)	170.2	Shale	0.24	0.05	0.05	0.85	1.19	1.62	0.73	0.71	15.2	6.49	5.91	25.68	3.55
Hongshuizhuang Fm.(J1)	182.5	Dolomite	0.15	0.03	0.00	0.30	0.48	1.00	0.48	0.63	0.29	3.61	6.53	0.44	1.78
Hongshuizhuang Fm.(J1)	183.6	Shale	0.11	0.15	0.03	1.11	1.39	2.42	0.57	0.80	3.74	3.81	7.75	4.83	1.59
Hongshuizhuang Fm.(J1)	189.6	Shale	0.19	0.04	0.02	0.58	0.83	1.14	0.73	0.70	2.34	2.99	4.73	4.95	2.04
Hongshuizhuang Fm.(J1)	192.9	Shale	0.27	0.05	0.04	1.01	1.37	1.85	0.74	0.74	22.8	6.21	5.17	44.08	3.87
Hongshuizhuang Fm.(J1)	200.6	Dolomite	0.08	0.02	0.01	0.42	0.53	1.09	0.48	0.79	5.50	3.29	5.70	9.65	1.86
Wumishan Fm.(J1)	217.8	Dolomite	0.71	0.06	0.06	0.04	0.87	1.93	0.45	0.04	0.14	0.44	4.62	0.31	0.31
Wumishan Fm.(J1)	245.0	Dolomite	0.05	0.02	0.00	0.14	0.21	0.30	0.71	0.66	0.43	0.34	0.57	7.60	1.96
Wumishan Fm.(J1)	251.0	Dolomite	0.08	0.02	0.00	0.09	0.19	0.26	0.73	0.46	0.64	0.56	0.42	15.05	4.31
Wumishan Fm.(J1)	261.5	Dolomite	0.12	0.02	0.00	0.03	0.18	0.28	0.64	0.17	0.11	0.23	0.39	2.92	1.96
Wumishan Fm.(J1)	268.9	Dolomite	0.14	0.01	0.00	0.01	0.16	0.26	0.60	0.04	0.12	0.23	0.15	7.76	4.81
Wumishan Fm.(J1)	283.6	Dolomite	0.13	0.02	0.01	0.00	0.17	0.25	0.66	0.01	0.06	0.28	0.19	3.16	4.60
Wumishan Fm.(J1)	305.5	Dolomite	0.06	0.01	0.00	0.09	0.17	0.26	0.63	0.57	0.09	0.58	0.24	3.79	7.79

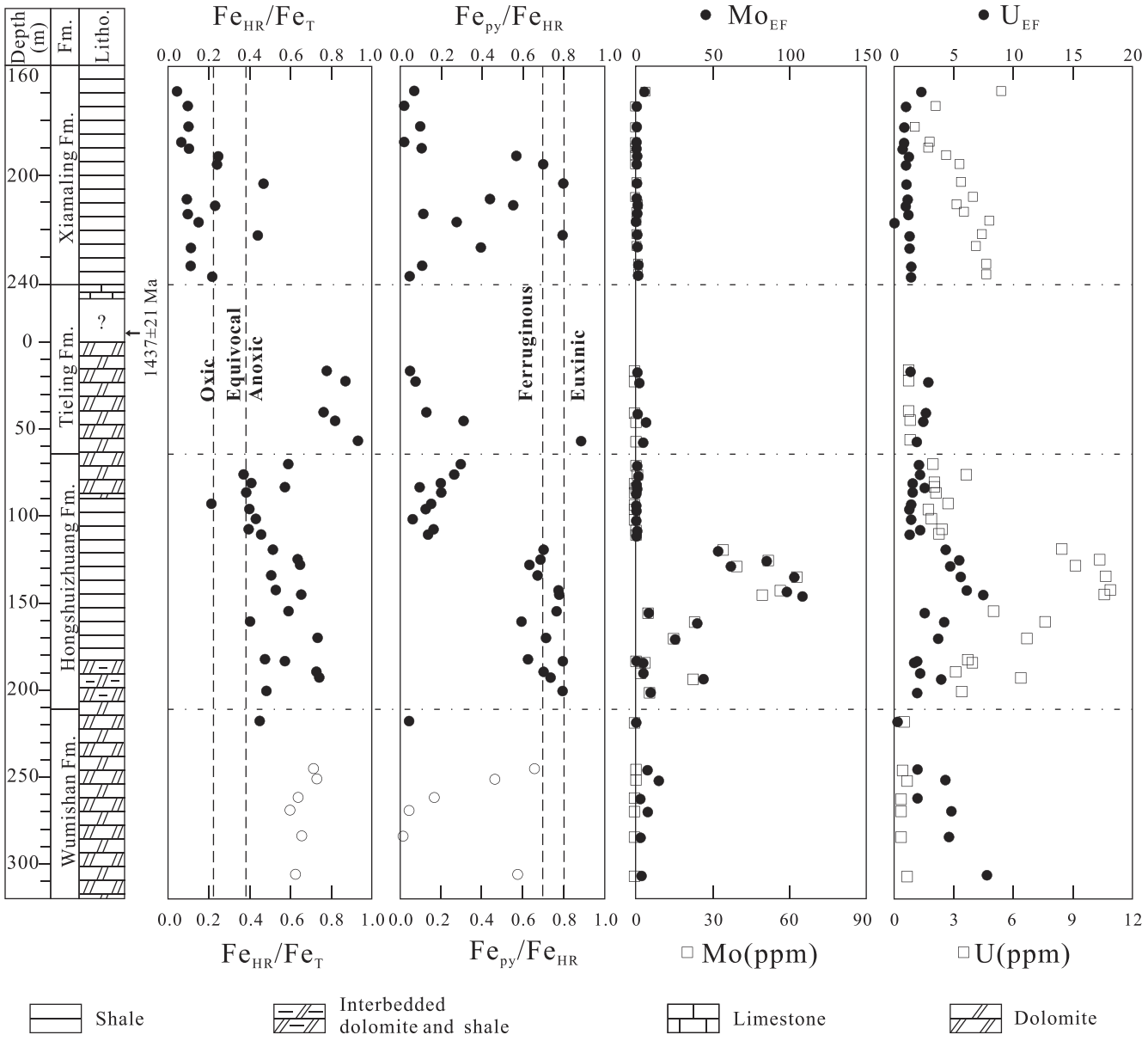

Fig. 3. Stratigraphic profiles of Fe species and trace metal enrichments for drill cores J1 and J2. For iron species data, the open circles represent samples with $Fe_T < 0.5\%$, and the closed circles represent samples with $Fe_T > 0.5\%$. For the trace metal data, the dots represent metal enrichment factors (Mo, U), and the open squares represent their abundances.

4. Results

4.1. Fe speciation

The iron speciation values are listed in Table 1 and illustrated in Figs. 2 and 3. In the Wumishan Formation, the Fe_{ox} and Fe_{mag} contents are generally low (< 0.1%), with Fe_{carb} and Fe_{py} ranging from 0.05% to 0.71% and from 0% to 0.14%, respectively (Fig. 2). Fe_T is generally lower than 0.3%, with one exception of 1.93% at 217.8 m, and the Fe_{HR}/Fe_T ratios all exceed 0.38 (Fig. 3). The Fe_{py}/Fe_{HR} ratios vary considerably and they decrease sharply from 0.57 at 305.5 m to 0.01 at 283.6 m (Fig. 3). After the decrease, the Fe_{py}/Fe_{HR} ratio increases gradually and peaks at 0.66 at 245 m, with a subsequent decline to 0.04 at 217.8 m (Fig. 3).

The Hongshuizhuang Formation shows distinct differences in Fe speciation data between the low-middle and upper intervals. In the lower-middle (200.6–119.7 m) Hongshuizhuang Formation, low Fe_{ox} and Fe_{mag} contents, with maximum values of 0.15% and 0.11%, respectively, are evident (Fig. 2). Fe_{carb} ranges from 0.08% to 0.45%, with Fe_{py} ranging from 0.30% to 1.53% (Fig. 2). The Fe_{HR}/Fe_T ratios are > 0.38, with high Fe_{py}/Fe_{HR} ratios from 0.6 to 0.8 (Fig. 3). In the upper Hongshuizhuang Formation (111.1–70.8 m), both the Fe_{ox} and Fe_{mag} contents are < 0.1%, with Fe_{carb} varying from 0.26% to 0.69% and with low Fe_{py} < 0.2% (Fig. 3). The Fe_{HR}/Fe_T ratios typically exceed 0.38, with a low value of 0.21 at 93.5 m (Fig. 3). The Fe_{py}/Fe_{HR} ratios range from 0.06 to 0.30 (Fig. 3).

In the Tieling Formation, the Fe_{ox} and Fe_{mag} contents are low (< 0.1%), similar to those in the Wumishan Formation. Fe_{carb} varies from 0.07% to 1.23%, with Fe_{py} ranging from 0.06% to 0.79% (Fig. 2). Fe_T ranges from 0.61% to 1.68% (Fig. 2). The Fe_{HR}/Fe_T ratios exceed 0.38, and Fe_{py}/Fe_{HR} mainly varies from 0.05 to 0.31, with a high value of 0.88 at 57.5 m (Fig. 3).

In the Xiamaling Formation, both Fe_{ox} and Fe_{mag} are much higher than in the Wumishan, Hongshuizhuang, and Tieling formations (Fig. 2). Fe_{ox} varies from 0.03% to 0.27%, with Fe_{mag} ranging from 0.02% to 0.91% (Fig. 2). Fe_{carb} and Fe_{py} fluctuate substantially, from

0.05% to 0.48%, and from 0.01% to 1.68%, respectively (Fig. 2). The Fe_{HR}/Fe_T ratios are < 0.38, ranging from 0.04 to 0.25, except for two ratios > 0.38 at the depths of 203.1 m and 222.0 m (Fig. 3). The Fe_{py}/Fe_{HR} ratios increase from 0.04 to 0.80 within the interval of 237.0–193.1 m and then remain roughly constant within the interval of 193.1–169.4 m, with an average of 0.06 (Fig. 3).

4.2. Trace elements (Mo, U)

In the Wumishan Formation, the Mo content is low (< 1 ppm), and the Mo_{EF} values range from 0.31 to 15.05 (Fig. 3). The U content is also low (< 1 ppm), with U_{EF} decreasing from 7.79 to 0.31 through the formation (Fig. 3).

In the lower-middle Hongshuizhuang Formation (200.6–119.7 m), the Mo content increases to 63 ppm, with high Mo_{EF} up to 108 (Fig. 3). The U content ranges from 3 ppm to 10.7 ppm, with relatively high U_{EF} reaching 7.3 (Fig. 3). In contrast, in the upper Hongshuizhuang Formation (111.1–70.8 m), the Mo content is < 1 ppm, with extremely low Mo_{EF} (< 2) (Fig. 3). The U content varies from 1.59 ppm to 3.47 ppm, and the U_{EF} values are also low with an average of 1.65 (Fig. 3).

In the Tieling Formation, the Mo and U contents are < 1 ppm, with Mo_{EF} and U_{EF} ranging from 1.1 to 6.7 and from 1.3 to 2.9, respectively (Fig. 3). In the Xiamaling Formation, there is a generally low Mo content (< 2 ppm) and Mo_{EF} (< 2) is present (Fig. 3). The U contents vary from 1.06 ppm to 5.44 ppm, with low U_{EF} (< 2) (Fig. 3).

5. Interpretation of stratigraphic variation in Fe chemistry and trace metal data

5.1. Wumishan Formation

The Wumishan Formation has relatively uniform Fe_{HR}/Fe_T ratios with an average of 0.63, which could result from an anoxic depositional environment (Figs. 3 and 4). Fe_{py} varies inversely with Fe_{carb}, with low ratios of Fe_{mag} and Fe_{ox} to Fe_{HR} (Fig. 2). Fe_{py}/Fe_{HR} varies mainly from 0.04 to 0.66 (Figs. 3 and 4) which is consistent with ferruginous bottom water conditions. However, the Wumishan carbonate contains extremely low Fe_T of 0.2–0.3%, except for a sample (J1-217.8) with Fe_T = 1.93% (Table 1). The low Fe_T (< 0.5%) could yield high Fe_{HR}/Fe_T ratios, which would suggest anoxic conditions, in contrast to evident oxic depositional conditions. Therefore, these samples with extremely low Fe_T may not provide reliable information about paleo-redox condition of ancient oceans (Clarkson et al., 2014; Raiswell et al., 2018).

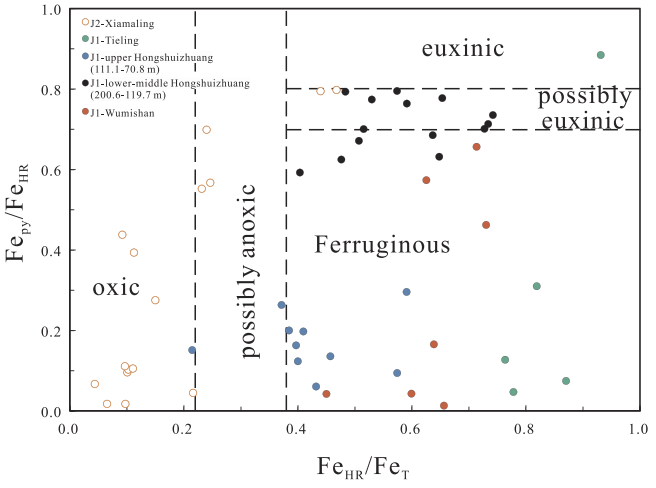

Fig. 4. Cross plot of Fe_{HR}/Fe_T vs. Fe_{py}/Fe_{HR} for the samples from each formation. The vertical lines intersect the x axis at Fe_{HR}/Fe_T ratios of 0.22 and 0.38, and the horizontal lines intersect the y axis the Fe_{py}/Fe_{HR} ratios of 0.7 and 0.8. Samples with Fe_{HR}/Fe_T > 0.38 and Fe_{py}/Fe_{HR} > 0.7 are probably deposited under euxinic conditions and samples with Fe_{HR}/Fe_T > 0.38 and Fe_{py}/Fe_{HR} < 0.7 deposit are probably deposited under anoxic and ferruginous conditions.

Mo_{EF} ranges from 1 to 10 in the Wumishan Formations (Table 1; Fig. 3). The relatively high U_{EF} and low Mo_{EF} could signal ferruginous conditions based on their absolute values. However, the Mo and U are both very low in Wumishan carbonate, and therefore the slightly high U_{EF} may be attributed to the low abundance of Al, mostly between 0.1 and 0.5% (in other words, authigenic enrichments are very low even if EFs are moderately elevated). Accordingly, the relatively high U_{EF} values are likely not of strong paleo-redox significance. From a sedimentological perspective, the Wumishan Formation consists mostly of shallow water carbonate as well as abundant stromatolites including various microdigitate structures with precipitate textures (Shi et al., 2008; Mei et al., 2010) which were likely formed and deposited under predominately oxic bottom water conditions (Guo et al., 2013). Further redox work on the Wumishan using proxies such as I/Ca or Ce anomalies will be useful in constraining the redox state of the overlying water column.

5.2. Hongshuizhuang Formation

The Fe speciation data vary substantially between the lower-middle Hongshuizhuang Formation (200.6–119.7 m) and upper Hongshuizhuang Formation (111.1–70.8 m) (Figs. 2 and 3). In the lower-middle Hongshuizhuang Formation, Fe_{py}/Fe_{HR} ranges from 0.6 to 0.8 accompanied by moderate changes in Fe_{HR}/Fe_T, indicating euxinic bottom water conditions (Figs. 3 and 4). The fraction of Fe_{carb} in Fe_{HR} decreases greatly, accompanied by a high content of Fe_{py}, reflecting euxinic conditions that contribute to the formation of pyrite (Fig. 2). This conclusion is supported by the trace metal data. High U_{EF} values reaching 7 in the lower Hongshuizhuang Formation indicate anoxic depositional conditions. In addition, high Mo_{EF}, with the maximum value of 108 (Fig. 3), supports the presence of free sulfide in the water column.

We note that the high Mo_{EF}, almost reaching those seen in modern sulfidic sediments, are not inconsistent with a low seawater Mo reservoir in middle Proterozoic oceans (Scott et al., 2008; Partin et al., 2013). Euxinic sediments in the Velkerri Formation, Roper Group, Australia, also record similar Mo concentrations of ~80 to 100 ppm (Nguyen et al., 2019; Cox et al., 2016). The Hongshuizhuang samples with Mo_{EF} > 35, have high Mo_{EF}/U_{EF} ratios > 3 × SW (seawater), which suggest intense redox cycling of metal-oxyhydroxides within the sulfidic water column also contributed to the Mo enrichments (Tribovillard et al., 2012).

In contrast to the lower-middle interval, the upper Hongshuizhuang Formation exhibits low Fe_{HR}/Fe_T ratios of ~0.38 with a minimum of 0.21, as well as low Fe_{py}/Fe_{HR} ratios < 0.3 with an average of 0.17 (Figs. 3 and 4). Taken together, the Fe speciation data suggest ferruginous depositional conditions for the upper Hongshuizhuang Formation (Figs. 3 and 4). The upper Hongshuizhuang Formation has extremely low Mo_{EF} (< 2) with low U_{EF} (Fig. 2), which can be attributed to low reservoirs of U and Mo in the Mesoproterozoic ocean combined with deposition under a ferruginous water column (Scott et al., 2008; Partin et al., 2013).

5.3. Tieling Formation

High Fe_{HR}/Fe_T ratios, with an average of 0.83, in the Tieling Formation, and Fe_{py}/Fe_{HR} ratios mainly ranging from 0.05 to 0.31, suggest predominantly ferruginous bottom water conditions (Figs. 3-4). However, a high Fe_{py}/Fe_{HR} of 0.88 at the depth of 57.5 m implies the occurrence of intermittent euxinia in the water column. The occurrence of ferruginous depositional conditions is supported by Ce anomalies

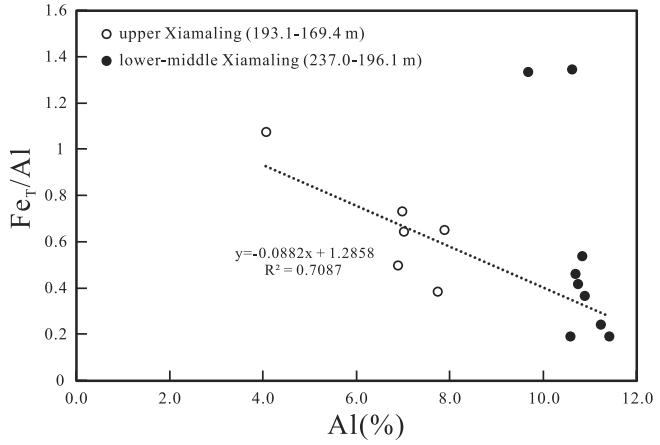

Fig. 5. Cross plot of Al content (%) vs. Fe_T/Al for the samples from the Xiamaling Formation.

(~1) from the Tieling Formation, which suggest anoxic conditions (Tang et al., 2017). Like the upper Hongshuizhuang Formation, low U_{EF} of < 3 combined with low Mo_{EF} (1–10) in the Tieling Formation suggests ferruginous deposition in basin whose seawater reservoirs of U and Mo were low.

5.4. Xiamaling Formation

The Xiamaling Formation has generally low Fe_{HR}/Fe_T ratios of < 0.25 with two high values of 0.47 and 0.44 (Fig. 3). The lower-middle Xiamaling Formation (237.0–196.1 m) are characterized by higher Fe_{py}, Fe_{HR}/Fe_T and Fe_{py}/Fe_{HR} ratios as well as Al abundance than the upper Xiamaling Formation (193.1–169.4 m) (Table 1 and Fig. 3). For the lower-middle Xiamaling Formation, except two high Fe_{HR}/Fe_T ratios, the low Fe_{HR}/Fe_T ratios with an average value of 0.17 could indicate oxic bottom water conditions (Figs. 3 and 4). However, Fe_T/Al, which has been considered as an indicator of Fe_{HR}, shows a negative correlation with Al content in Xiamaling Formation except two samples (J2-233.1 and J2-214.2) (Fig. 5). The Al contents vary from 11.42% to 9.69% in the lower-middle Xiamaling Formation, and therefore, the plot between Fe_T/Al and the high Al contents of the lower-middle Xiamaling Formation suggest that the enrichment of Fe_{HR} could be diluted by siliciclastic input (Lyons and Severmann, 2006). Though the true Fe_{HR}/Fe_T ratios remain unknown, the high pyrite content, stratigraphic increase of Fe_{py}/Fe_{HR} as well as relatively high U_{EF} suggest that the lower-middle Xiamaling Formation was possibly deposited under anoxic conditions. The two samples with high Fe_{py}/Fe_{HR} ratios of ~0.8 with Fe_{HR}/Fe_T > 0.38 suggest transient euxinic conditions when the lower-middle Xiamaling was deposited (Figs. 3 and 4). By contrast, the low Fe_{py} ranging from 0.01 to 0.05%, low Fe_{HR}/Fe_T ratio from 0.04 to 0.10, low Fe_{py}/Fe_{HR} ratio from 0.02 to 0.10 as well as low Mo_{EF} and U_{EF} with relatively low Al content from 4.07 to 7.90% provide strong evidence of oxic bottom water conditions when the upper Xiamaling was deposited (Fig. 3).

As discussed above, low Fe_{HR}/Fe_T ratios (< 0.38) were also reported from the mid-upper Xiamaling Formation (Units 2 and 3) and were interpreted to have resulted from oxic depositional conditions (Zhang et al., 2016a, 2017, 2019). Based on the Xiamaling data, it was hypothesized that the atmospheric oxygen level may have been ≥ 3.8% PAL, which may be sufficient for animal respiration (Zhang et al., 2016a, 2017, 2019). However, Diamond et al. (2018) attributed low Fe_{HR}/Fe_T ratios (< 0.38) from the Xiamaling Formation to an insufficient source of Fe_{HR}. They argued that it was the reservoir size rather than oxic conditions that resulted in low Fe_{HR}/Fe_T ratios and low trace metal enrichment. As such, Diamond et al. (2018) challenged the hypothesis of an atmospheric oxygen level of ≥ 3.8% PAL estimated by Zhang et al. (2016a) (see also Planavsky et al., 2016; Zhang et al., 2016b).

The Xiamaling Formation samples from drill core J2 in this study may be correlative with Unit 6 in the Xiahuayuan region and stratigraphically they might be more than 200 m below the Units 2 and 3 studied by Wang et al. (2017). Our Fe speciation and trace metal data suggest possible anoxic depositional conditions with transient euxinic conditions during the deposition of lower-middle Xiamaling Formation and predominately oxic bottom water conditions when the upper Xiamaling Formation was deposited. Our results show that the paleo-redox conditions during the deposition of the Xiamaling Formation may have varied greatly throughout the formation.

6. Global paleo-redox heterogeneity in Mesoproterozoic oceans

A compilation of the published Fe speciation data for the Mesoproterozoic worldwide reveals that our Fe speciation data from the Yanshan Basin help fill a global data gap from 1500 Ma to 1400 Ma (Fig. 6A). Most of the Fe_{HR}/Fe_T ratios suggest anoxic conditions for the middle Proterozoic oceans (Fig. 6B), and by inference an atmospheric oxygen level that was likely lower than Modern. In the compilation, the highest density in the heat map is the red area of Fe_{HR}/Fe_T ~ 0.2 (Fig. 7A), however, most samples still have Fe_{HR}/Fe_T > 0.38, which suggest anoxic conditions (Fig. 7B). The low density of the samples with Fe_{HR}/Fe_T > 0.38 may result from a larger space area of the anoxic conditions on the bivariate plot (Fig. 7A). Fe_{py}/Fe_{HR} ratios are mainly < 0.7, suggesting the occurrence of dominantly ferruginous conditions (Fig. 7B). Abundant data with Fe_{HR}/Fe_T > 0.38 and Fe_{py}/Fe_T > 0.7 are observed, indicating sulfidic bottom water conditions (Fig. 7B). Therefore, although ferruginous conditions are suggested to have been predominant during the mid-Proterozoic, the data indicate that euxinic conditions were also not uncommon in sampled formations (Fig. 7), suggesting a complex paleo-redox structure of the mid-Proterozoic oceans. We also compiled published Fe_{HR}/Fe_T and Fe_{py}/Fe_{HR} ratios and their number of occurrences, which are illustrated in Fig. 7B; they clearly indicate heterogenous redox conditions in the global mid-Proterozoic oceans, consistent with the previous studies.

Intriguingly, the results show a high proportion of samples plotting in the 'oxic' field, or more specifically having low Fe_{HR}/Fe_T ratios (Fig. 7). While it is true that all samples in the modern oxic baseline dataset have Fe_{HR}/Fe_T < 0.38 (Raiswell and Canfield, 1998), and no modern anoxic sample has Fe_{HR}/Fe_T < 0.2 (or in other words, only oxic samples have Fe_{HR}/Fe_T < 0.2—see discussion in Sperling et al., 2016), interpretation of iron speciation data is inherently asymmetric. Identification of elevated Fe_{HR}/Fe_T 'unequivocally' identifies sedimentation under an anoxic water column, whereas low Fe_{HR}/Fe_T simply indicates the absence of substantial authigenic Fe_{HR} enrichment. This lack of enrichment could result from 1) sedimentation under an oxygenated water column, such that all Fe_{HR} is delivered through detrital processes, 2) under an anoxic water column, but with rapid sedimentation, such that there is not enough time for authigenic enrichments to accumulate, 3) very widespread anoxic conditions (due to mass balance constraints, not all areas can be 'enriched' if an ocean is dominantly anoxic), or 4) if iron released during early diagenesis is being sequestered in clay minerals not extracted in the standard sequential extraction procedure (see discussion in Doyle et al., 2018). Considering this, one possibility based on the standard interpretative framework of Fe speciation data is that the occurrence of oxic environments may have been underestimated in the Mesoproterozoic. Given that rapid sedimentation is unlikely to have affected all these shale formations (and most show no evidence for very rapid sedimentation), we can rule out the second possibility as a global driver of this signal. The third and fourth possibilities—non-uniformitarian iron cycling during the Mesoproterozoic—represent a more likely alternative scenario. Although the compilation here cannot uniquely distinguish between these two possibilities of more widespread oxic

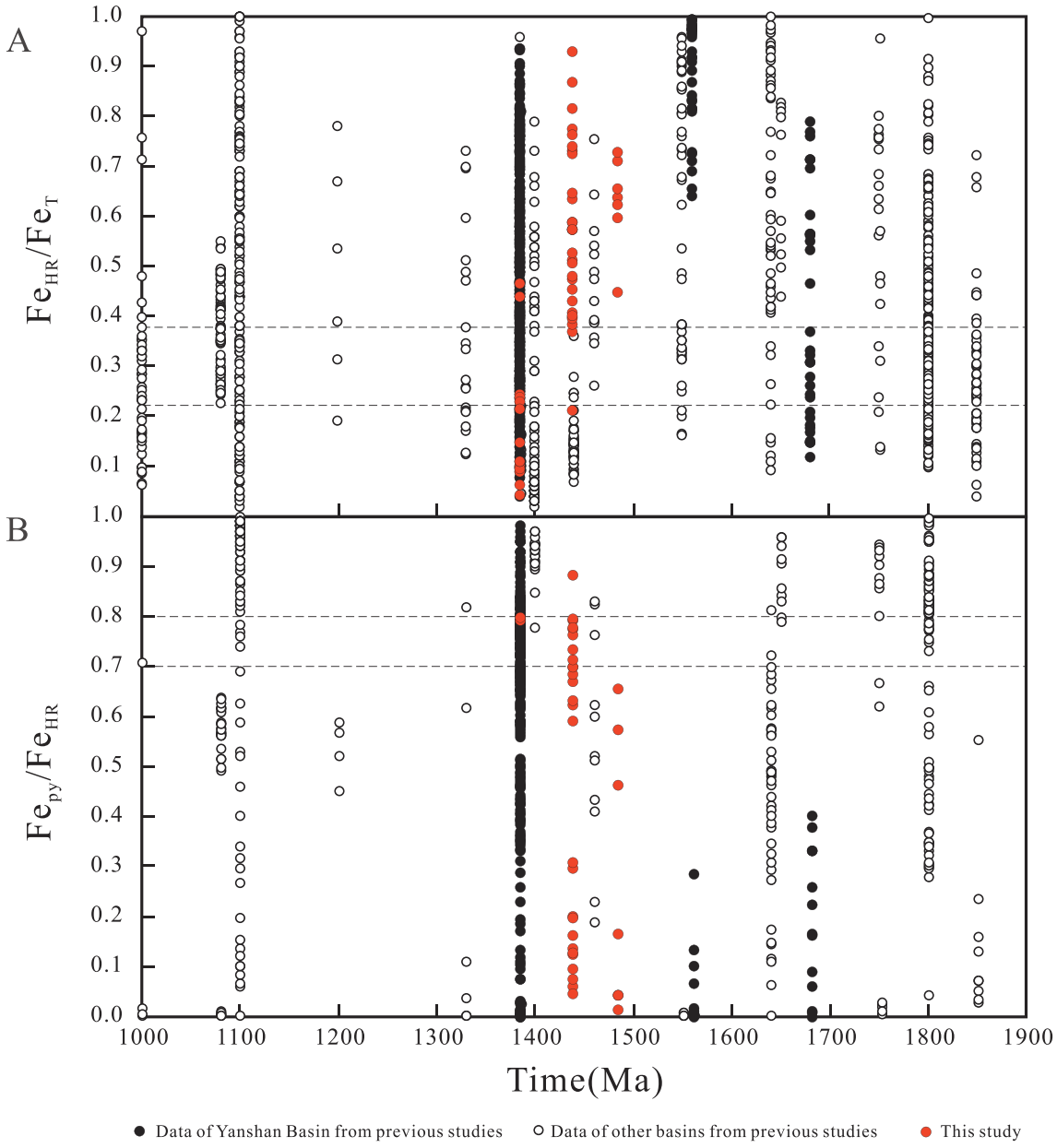

Fig. 6. Times series of Fe species from 1800 Ma to 1000 Ma (Shen et al., 2002, 2003; Poulton et al., 2010; Planavsky et al., 2011, 2018; Geboy et al., 2013; Gilleaudeau and Kah, 2013; Sperling et al., 2014, 2015; Zhang et al., 2016a, 2017, 2019; Wang et al., 2017; Diamond et al., 2018; Doyle et al., 2018; Zhang et al., 2018). (A): Time series of Fe_{HR}/Fe_T. When $Fe_{HR}/Fe_T > 0.38$, shown by the upper dashed line, anoxic conditions are suggested. (B): Time series of Fe_{py}/Fe_{HR} for samples with $Fe_{HR}/Fe_T > 0.38$. Euxinic conditions are indicated when $Fe_{py}/Fe_{HR} > 0.7$, shown by the lower dashed line, and the ratio < 0.7 suggests ferruginous conditions.

conditions than generally considered or non-uniformitarian iron cycling, the proportion of "oxic"/low Fe_{HR}/Fe_T samples contrasts with data generated from Neoproterozoic and Paleozoic shale successions (Sperling et al., 2015).

These distinctly contrasting interpretations have important implications for biological evolution at this time. Specifically, redox conditions of Earth's surface environments may have significant implications for the evolution of complex eukaryotes. Although it has recently been recognized that the oxygen requirements of many Mesoproterozoic eukaryotes may be lower than generally considered (Porter et al., 2018), oxygenation is still considered as one of critical environmental contributors for the evolution of complex, multicellular eukaryotes. Although the exact oxygen levels are debated, higher oxygen levels are certainly required to support the activities of eukaryotes with large bodies and more complex food webs (Sperling et al., 2013; Cole et al., 2020).

7. Conclusions

Integrated with trace metal (U and Mo) data, the Fe speciation data reported in this study reveal significant redox variations from mainly anoxic conditions to likely oxic conditions in the Yanshan Basin during ~1500 to 1380 Ma. The Fe speciation data also help distinguish ferruginous conditions from sulfidic bottom water conditions. The new data from the Wumishan and Tieling formations suggest that they may have deposited under oxic and ferruginous conditions, respectively (although the redox proxies used here, mainly designed for use in shales, may not be applicable to the Wumishan Formation). Redox conditions varied from euxinic conditions in the lower-middle Hongshuizhuang Formation to ferruginous conditions in the upper

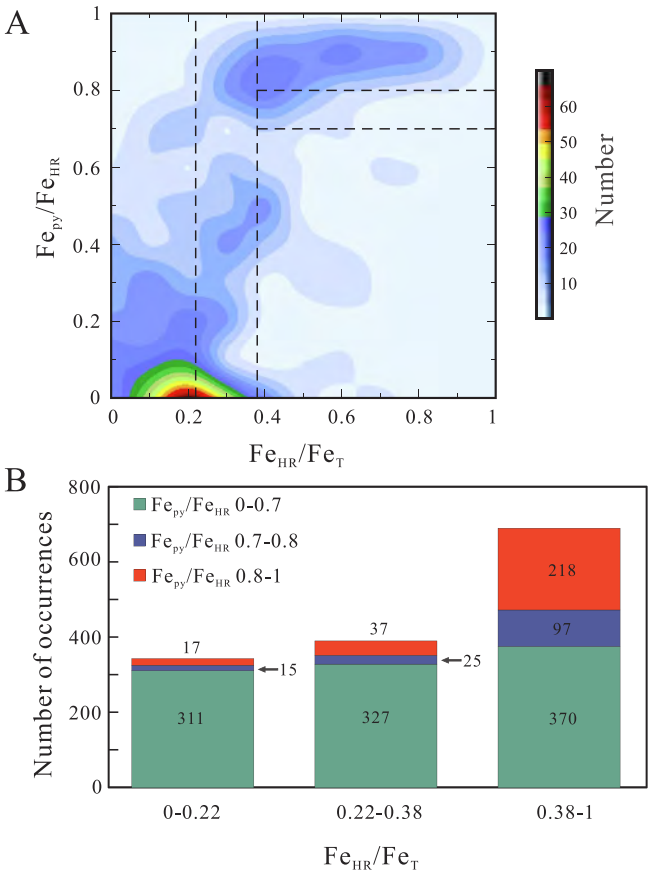

Fig. 7. (A). Heat map of Fe_{HR}/Fe_T vs. Fe_{py}/Fe_{HR} for samples from 1800 Ma to 1000 Ma. The colors represent the density of the data set as the color bar describe. The numbers on the color bar represent the number of occurrences in a square unit with side length of 0.01. (B). The number of occurrences for different ranges of Fe_{HR}/Fe_T and Fe_{py}/Fe_{HR}. Likely oxic conditions refer to $Fe_{HR}/Fe_T < 0.22$. Ferruginous conditions refer to $Fe_{HR}/Fe_T > 0.38$ with $Fe_{py}/Fe_{HR} < 0.7$, and euxinic conditions refer to $Fe_{HR}/Fe_T > 0.38$ with $Fe_{py}/Fe_{HR} > 0.7$.

Hongshuizhuang Formation. The Fe speciation data from the lower-middle Xiamaling Formation suggest possible anoxic bottom water conditions with transient euxinic conditions and that the upper Xiamaling Formation was probably deposited under oxic bottom water conditions.

The compilation of the Fe species from Mesoproterozoic basins suggests that oxic environments may have been underestimated. Ferruginous conditions could have been dominant in the deeper basins, although euxinic conditions were not uncommon. Determining the causes behind the high proportion of low Fe_{HR}/Fe_T samples in the Mesoproterozoic, and better identifying the oxygenation history of this era, will be key to tracking potentially favorable habitat for early eukaryotes.

Declaration of Competing Interest

The authors declare that they have no known competing financial interests or personal relationships that could have appeared to influence the work reported in this paper.

Acknowledgements

This study was supported by National Natural Science Foundation of China (41721002, 41520104007, 41890842, 41922021), the “111” project, and the Chinese Academy of Sciences (QYZDY-SSW-DQC031).

We thank Linda C. Kah and an anonymous reviewer for constructive comments that have greatly improved this study.

References

Anbar, A.D., Duan, Y., Lyons, T.W., Arnold, G.L., Kendall, B., Creaser, R.A., Kaufman, A.J., Gordon, G.W., Scott, C., Garvin, J., Buick, R., 2007. A whiff of oxygen before the great oxidation event? Science 317, 1903–1906.
Anbar, A.D., Knoll, A.H., 2002. Proterozoic ocean chemistry and evolution: a bioinorganic bridge? Science 297, 1137–1142.
Anderson, R.F., Fleisher, M.Q., Lehuray, A.P., 1989. Concentration, oxidation-state, and particulate flux of uranium in the Black Sea. Geochim. Cosmochim. Acta 53, 2215–2224.
Arnold, G.L., Anbar, A.D., Barling, J., Lyon, T.W., 2004. Molybdenum isotope evidence for widespread anoxia in mid-Proterozoic oceans. Science 304, 87–90.
Bartley, J.K., Kah, L.C., 2004. Marine carbon reservoir, C_{org}-C_{carb} coupling, and the evolution of the Proterozoic carbon cycle. Geology 32, 129–132.
Buick, R., Marais, D.J.D., Knoll, A.H., 1995. Stable isotopic compositions of carbonates from the Mesoproterozoic Bangemall Group, northwestern Australia. Chem. Geol. 123, 153–171.
Butterfield, N.J., 2015. Early evolution of the Eukaryota. Palaeontology 58, 5–17.
Calvert, S.E., Pedersen, T.F., 1993. Geochemistry of recent oxic and anoxic marine sediments: implications for the geological record. Marine Geol. 113, 67–88.
Canfield, D.E., 1998. A new model for Proterozoic ocean chemistry. Nature 396, 450–453.
Canfield, D.E., Raiswell, R., Westrich, J.T., Reaves, C.M., Berner, R.A., 1986. The use of chromium reduction in the analysis of reduced inorganic sulfur in sediments and shales. Chem. Geol. 54, 149–155.
Clarkson, M.O., Poulton, S.W., Guilbaud, R., Wood, R.A., 2014. Assessing the utility of Fe/Al and Fe-speciation to record water column redox conditions in carbonate-rich sediments. Chem. Geol. 382, 111–122.
Cohen, P.A., Macdonald, F.A., 2015. The Proterozoic record of eukaryotes. Paleobiology 41, 610–632.
Cole, D.B., Mills, D.B., Erwin, D.H., Sperling, E.A., Porter, S.M., Reinhard, C.T., Planavsky, N.J., 2020. On the coevolution of surface oxygen levels and animals. Geobiology 00, 1–22.
Cox, G.M., Jarrett, A., Edwards, D., Crockford, P.W., Halverson, G.P., Collins, A.S., Poirier, A., Li, Z., 2016. Basin redox and primary productivity within the Mesoproterozoic Roper Seaway. Chem. Geol. 440, 101–114.
Crockford, P.W., Hayles, J.A., Bao, H., Planavsky, N.J., Bekker, A., Fralick, P.W., Halverson, G.P., Bui, T.H., Peng, Y., Wing, B.A., 2018. Triple oxygen isotope evidence for limited mid-Proterozoic primary productivity. Nature 559, 613–616.
Crockford, P.W., Kunzmann, M., Bekker, A., Hayles, J., Bao, H., Halverson, G.P., Peng, Y., Bui, T.H., Cox, G.M., Gibson, T.M., Wörndle, S., Rainbird, R., Lepland, A., Swanson-Hysell, N.L., Master, S., Sreenivas, B., Kuznetsov, A., Krupenik, V., Wing, B.A., 2019. Claypool continued: extending the isotopic record of sedimentary sulfate. Chem. Geol. 513, 200–225.
Diamond, C.W., Planavsky, N.J., Wang, C., Lyons, T.W., 2018. What the similar to 1.4 Ga Xiamaling Formation can and cannot tell us about the mid-Proterozoic ocean. Geobiology 16, 219–236.
Doyle, K.A., Poulton, S.W., Newton, R.J., Podkovyrov, V.N., Bekker, A., 2018. Shallow water anoxia in the Mesoproterozoic ocean: Evidence from the Bashkir Meganticlinorium, Southern Urals. Precambr. Res. 317, 196–210.
Farquhar, J., Bao, H.M., Thiemens, M.H., 2000. Atmospheric influence of Earth's earliest sulfur cycle. Science 289, 756–758.
Geboy, N.J., Kaufman, A.J., Walker, R.J., Misi, A., de Oliviera, T.F., Miller, K.E., Azmy, K., Kendall, B., Poulton, S.W., 2013. Re-Os age constraints and new observations of Proterozoic glacial deposits in the Vazante Group, Brazil. Precambr. Res. 238, 199–213.
Gilleaudeau, G.J., Frei, R., Kaufman, A.J., Kah, L.C., Azmy, K., Bartley, J.K., Chernyavskiy, P., Knoll, A.H., 2016. Oxygenation of the mid-Proterozoic atmosphere: clues from chromium isotopes in carbonates. Geochem. Perspect. Lett. 2, 178–187.
Gilleaudeau, G.J., Kah, L.C., 2013. Oceanic molybdenum drawdown by epeiric sea expansion in the Mesoproterozoic. Chem. Geol. 356, 21–37.
Gilleaudeau, G.J., Kah, L.C., 2015. Heterogeneous redox conditions and a shallow chemocline in the Mesoproterozoic ocean: Evidence from carbon-sulfur-iron relationships. Precambr. Res. 257, 94–108.
Gilleaudeau, G.J., Romaniello, S.J., Luo, G., Kaufman, A.J., Zhang, F., Klaebe, R.M., Kah, L.C., Azmy, K., Bartley, J.K., Zheng, W., Knoll, A.H., Anbar, A.D., 2019. Uranium isotope evidence for limited euxinia in mid-Proterozoic oceans. Earth Planet. Sci. Lett. 521, 150–157.
Grotzinger, J.P., Knoll, A.H., 1999. Stromatolites in Precambrian carbonates: evolutionary mileposts or environmental dipsticks? Annu. Rev. Earth Planet. Sci. 27, 313–358.
Guo, H., Du, Y., Kah, L.C., Hu, C., Huang, J., Hu, H., Yu, W., Song, H., 2015. Sulfur isotope composition of carbonate-associated sulfate from the Mesoproterozoic Jixian Group, North China: implications for the marine sulfur cycle. Precambr. Res. 266, 319–336.
Guo, H., Du, Y., Kah, L.C., Huang, J., Hu, C., Hu, H., Yu, W., 2013. Isotopic composition of organic and inorganic carbon from the Mesoproterozoic Jixian Group, North China: implications for biological and oceanic evolution. Precambr. Res. 224, 169–183.
Helz, G.R., Miller, C.V., Charnock, J.M., Mosselmans, J.F.W., Pattrick, R.A.D., Garner, C.D., Vaughan, D.J., 1996. Mechanism of molybdenum removal from the sea and its concentration in black shales: EXAFS evidence. Geochim. Cosmochim. Acta 60, 3631–3642.
Kah, L.C., Bartley, J.K., 2011. Protracted oxygenation of the Proterozoic biosphere.

Intern. Geol. Rev. 53, 1424–1442.
Kah, L.C., Knoll, A.H., 1996. Microbenthic distribution of Proterozoic tidal flats: environmental and taphonomic considerations. Geology 24, 79–82.
Kah, L.C., Lyons, T.W., Chesley, J.T., 2001. Geochemistry of a 1.2 Ga carbonate-evaporites succession, northern Baffin Island: implications for Mesoproterozoic marine evolution. Precambr. Res. 111, 203–234.
Kah, L.C., Lyons, T.W., Frank, T.D., 2004. Low marine sulphate and protracted oxygenation of the Proterozoic biosphere. Nature 431, 834–838.
Kah, L.C., Sherman, A.G., Narbonne, G.M., Knoll, A.H., Kaufman, A.J., 1999. $\delta^{13}C$ stratigraphy of the Proterozoic Bylot Supergroup, Baffin Island, Canada: implications for regional lithostratigraphic correlations. Canadian J. Earth Sci. 36, 313–332.
Kendall, B., Gordon, G.W., Poulton, S.W., Anbar, A.D., 2011. Molybdenum isotope constraints on the extent of late Paleoproterozoic ocean euxinia. Earth Planet. Sci. Lett. 307, 450–460.
Li, H., Su, W., Zhou, H., Xiang, Z., Tian, H., Yang, L., Huff, D.W., Ettensohn, R.F., 2014. The first precise age constraints on the Jixian System of the Meso- to Neoproterozoic Standard Section of China: SHRIMP zircon U-Pb dating of bentonites from the Wumishan and Tieling formations in the Jixian Section, North China Craton. Acta Petrol. Sin. 30, 2999–3012.
Liu, Y., Zong, K., Kelemen, P.B., Gao, S., 2008. Geochemistry and magmatic history of eclogites and ultramafic rocks from the Chinese continental scientific drill hole: subduction and ultrahigh-pressure metamorphism of lower crustal cumulates. Chem. Geol. 247, 133–153.
Lu, S., Zhao, G., Wang, H., Hao, G., 2008. Precambrian metamorphic basement and sedimentary cover of the North China Craton: a review. Precambr. Res. 160, 77–93.
Luo, G., Junium, C.K., Kump, L.R., Huang, J., Li, C., Feng, Q., Shi, X., Bai, X., Xie, S., 2014. Shallow stratification prevailed for ~1700 to ~1300Ma ocean: Evidence from organic carbon isotopes in the North China Craton. Earth Planet. Sci. Lett. 400, 219–232.
Luo, G., Ono, S., Huang, J., Algeo, T.J., Li, C., Zhou, L., Robinson, A., Lyons, T.W., Xie, S., 2015. Decline in oceanic sulfate levels during the early Mesoproterozoic. Precambr. Res. 258, 36–47.
Luo, Q., Zhong, N., Lei, Z., Wang, Y., Jing, Q., Lin, Q., Yi, Z., Yong, M., 2013. Correlation of burial organic carbon and paleoproductivity in the Mesoproterozoic Hongshuizhuang Formation, northern North China. Chin. Sci. Bull. 58, 1299–1309.
Lyons, T.W., Severmann, S., 2006. A critical look at iron paleoredox proxies: new insights from modern euxinic marine basins. Geochim. Cosmochim. Acta 70, 5698–5722.
McManus, J., Berelson, W.M., Klinkhammer, G.P., Hammond, D.E., Holm, C., 2005. Authigenic uranium: relationship to oxygen penetration depth and organic carbon rain. Geochim. Cosmochim. Acta 69, 95–108.
Mei, M., Gao, J., Meng, Q., Liu, Z., 2010. Sedimentary features and their implications of microdigital stromatolites from the Mesoproterozoic Wumishan Formation at the Jixian section in North China. Acta Geol. Sin. 84, 483–496.
Mei, M., Yang, F., Gao, J., Meng, Q., 2008. Glauconites formed in the high-energy shallow-marine environment of the Late Mesoproterozoic: case study from Tieling Formation at Jixian Section in Tianjin, North China. Earth Sci. Front. 15, 146–158.
Morford, J.L., Martin, W.R., Francois, R., Carney, C.M., 2009. A model for uranium, rhenium, and molybdenum diagenesis in marine sediments based on results from coastal locations. Geochim. Cosmochim. Acta 73, 2938–2960.
Nguyen, K., Love, G.D., Zumberge, J.A., Kelly, A.E., Owens, J.D., Rohrssen, M.K., Bates, S.M., Cai, C., Lyons, T.W., 2019. Absence of biomarker evidence for early eukaryotic life from the Mesoproterozoic Roper Group: Searching across a marine redox gradient in mid-Proterozoic habitability. Geobiology 17, 247–260.
Parnell, J., Boyce, A.J., Mark, D., Bowden, S., Spinks, S., 2010. Early oxygenation of the terrestrial environment during the Mesoproterozoic. Nature 468, 290–293.
Partin, C.A., Bekker, A., Planavsky, N.J., Scott, C.T., Gill, B.C., Li, C., Podkovyrov, V., Maslov, A., Konhauser, K.O., Lalonde, S.V., Love, G.D., Poulton, S.W., Lyons, T.W., 2013. Large-scale fluctuations in Precambrian atmospheric and oceanic oxygen levels from the record of U in shales. Earth Planet. Sci. Lett. 369, 284–293.
Planavsky, N.J., Cole, D.B., Reinhard, C.T., Diamond, C., Love, G.D., Luo, G., Zhang, S., Konhauser, K.O., Lyons, T.W., 2016. No evidence for high atmospheric oxygen levels 1,400 million years ago. Proc. Natl. Acad. Sci. 113, E2550–E2551.
Planavsky, N.J., McGoldrick, P., Scott, C.T., Li, C., Reinhard, C.T., Kelly, A.E., Chu, X.L., Bekker, A., Love, G.D., Lyons, T.W., 2011. Widespread iron-rich conditions in the mid-Proterozoic ocean. Nature 477, 448–451.
Planavsky, N.J., Reinhard, C.T., Wang, X.L., Thomson, D., McGoldrick, P., Rainbird, R.H., Johnson, T., Fischer, W.W., Lyons, T.W., 2014. Low Mid-Proterozoic atmospheric oxygen levels and the delayed rise of animals. Science 346, 635–638.
Planavsky, N.J., Slack, J.F., Cannon, W.F., O'Connell, B., Isson, T.T., Asael, D., Jackson, J.C., Hardisty, D.S., Lyons, T.W., Bekker, A., 2018. Evidence for episodic oxygenation in a weakly redox-buffered deep mid-Proterozoic ocean. Chem. Geol. 483, 581–594.
Pollock, M.D., Kah, L.C., Bartley, J.K., 2006. Morphology of molar-tooth structures in Precambrian carbonates: influence of substrate rheology and implications for genesis. J. Sediment. Res. 76, 310–323.
Porter, S.M., Agić, H., Riedman, L.A., 2018. Anoxic ecosystems and early eukaryotes. Emerg. Top. Life Sci. 2, 299–309.
Poulton, S.W., Canfield, D.E., 2005. Development of a sequential extraction procedure for iron: implications for iron partitioning in continentally derived particulates. Chem. Geol. 214, 209–221.
Poulton, S.W., Fralick, P.W., Canfield, D.E., 2004. The transition to a sulphidic ocean approximately 1.84 billion years ago. Nature 431, 173–177.
Poulton, S.W., Fralick, P.W., Canfield, D.E., 2010. Spatial variability in oceanic redox structure 1.8 billion years ago. Nat. Geosci. 3, 486–490.
Qiao, X., Gao, L., Zhang, C., 2007. The Meso- and Neoproterozoic chronostratigraphic chart and tectonic environment in Sino-Korean Plate. Geol. Bull. China 26, 503–509 (in Chinese with English abstract).
Raiswell, R., Canfield, D.E., 1998. Sources of iron for pyrite formation in marine sediments. Am. J. Sci. 298, 219–245.
Raiswell, R., Hardisty, D.S., Lyons, T.W., Canfield, D.E., Reinhard, C.T., 2018. The iron paleoredox proxies: a guide to the pitfalls, problems and proper practice. Am. J. Sci. 318, 491–526.
Reinhard, C.T., Planavsky, N.J., Robbins, L.J., Partin, C.A., Gill, B.C., Lalonde, S.V., Bekker, A., Konhauser, K.O., Lyons, T.W., 2013. Proterozoic ocean redox and biogeochemical stasis. Proc. Natl. Acad. Sci. 110, 5357–5362.
Rice, C.A., Tuttle, M.L., Reynolds, R.L., 1993. The analysis of forms of sulfur in ancient sediments and sedimentary rocks: comments and cautions. Chem. Geol. 107, 83–95.
Scott, C., Lyons, T.W., Bekker, A., Shen, Y., Poulton, S.W., Chu, X., Anbar, A.D., 2008. Tracing the stepwise oxygenation of the Proterozoic ocean. Nature 452, 456–459.
Shang, M., Tang, D., Shi, X., Zhou, L., Zhou, X., Song, H., Jiang, G., 2019. A pulse of oxygen increase in the early Mesoproterozoic ocean at ca. 1.57-1.56 Ga. Earth Planet. Sci. Lett. 527, 115797.
Shen, Y., Canfield, D.E., Knoll, A.H., 2002. Middle Proterozoic ocean chemistry: evidence from the McArthur Basin, northern Australia. Am. J. Sci. 302, 81–109.
Shen, Y., Knoll, A.H., Walter, M.R., 2003. Evidence for low sulphate and anoxia in a mid-Proterozoic marine basin. Nature 423, 632–635.
Shi, Z., Zhang, C., Jiang, G., Liu, J., Wang, Y., Liu, D., 2008. Microbial mats in the Mesoproterozoic carbonates of the North China Platform and their potential for hydrocarbon generation. J. China Univ. Geosci. 19, 549–566.
Shields, G.A., 2002. "Molar-tooth microspar": a chemical explanation for its disappearance ~750 Ma. Terra Nova 14, 108–113.
Slotznick, S.P., Sperling, E.A., Tosca, N.J., Miller, A.J., Clayton, K., van Helmond, N.A.G.M., Slomp, C.P., Swanson-Hysell, N.L., 2020. Unraveling the mineralogical complexity of sediment iron speciation using sequential extractions. Geochemistry, Geophysics, Geosystems 21, e2019GC008666.
Slotznick, S.P., Swanson-Hysell, N.L., Sperling, E.A., 2018. Oxygenated Mesoproterozoic lake revealed through magnetic mineralogy. Proc. Natl. Acad. Sci. 115, 12938–12943.
Sperling, E.A., Carbone, C., Strauss, J.V., Johnston, D.T., Narbonne, G.M., Macdonald, F.A., 2016. Oxygen, facies, and secular controls on the appearance of Cryogenian and Ediacaran body and trace fossils in the Mackenzie Mountains of northwestern Canada. Geol. Soc. Am. Bull. 128, 558–575.
Sperling, E.A., Frieder, C.A., Raman, A.V., Girguis, P.R., Levin, L.A., Knoll, A.H., 2013. Oxygen, ecology, and the Cambrian radiation of animals. Proc. Natl. Acad. Sci. 110, 13446–13451.
Sperling, E.A., Rooney, A.D., Hays, L., Sergeev, V.N., Vorob'eva, N.G., Sergeeva, N.D., Selby, D., Johnston, D.T., Knoll, A.H., 2014. Redox heterogeneity of subsurface waters in the Mesoproterozoic ocean. Geobiology 12, 373–386.
Sperling, E.A., Wolock, C.J., Morgan, A.S., Gill, B.C., Marcus, K., Halverson, G.P., Macdonald, F.A., Knoll, A.H., Johnston, D.T., 2015. Statistical analysis of iron geochemical data suggests limited late Proterozoic oxygenation. Nature 523, 451–454.
Stookey, L.L., 1970. Ferrozine-a new spectrophotometric reagent for iron. Anal. Chem. 42, 779–781.
Su, W., Li, H., Huff, W.D., Ettensohn, F.R., Zhang, S., Zhou, H., Wan, Y., 2010. SHRIMP U-Pb dating for a K-bentonite bed in the Tieling Formation, North China. Chin. Sci. Bull. 55, 3312–3323.
Su, W., Zhang, S., Huff, W.D., Li, H., Ettensohn, F.R., Chen, X., Yang, H., Han, Y., Song, B., Santosh, M., 2008. SHRIMP U-Pb ages of K-bentonite beds in the Xiamaling Formation: implications for revised subdivision of the Meso- to Neoproterozoic history of the North China Craton. Gondwana Res. 14, 543–553.
Tang, D., Shi, X., Ma, J., Jiang, G., Zhou, X., Shi, Q., 2017. Formation of shallow-water glaucony in weakly oxygenated Precambrian ocean: an example from the mesoproterozoic tieling formation in North China. Precambr. Res. 294, 214–229.
Taylor, S.R., McLennan, S.M., 1985. The Continental Crust: Its Composition and Evolution. Blackwell Scientific, Oxford, pp. 312.
Tribovillard, N., Algeo, T.J., Baudin, F., Riboulleau, A., 2012. Analysis of marine environmental conditions based on molybdenum-uranium covariation-applications to Mesozoic paleoceanography. Chem. Geol. 324, 46–58.
Tribovillard, N., Algeo, T.J., Lyons, T., Riboulleau, A., 2006. Trace metals as paleoredox and paleoproductivity proxies: an update. Chem. Geol. 232, 12–32.
Wang, L., Li, B., 1993. Sedimentary sequences and source beds in the Xiamaling formation in Northwestern Hebei. Lithofacies Palaeogeogr. 13, 38–45 (in Chinese).
Wang, X., Zhang, S., Wang, H., Bjerrum, C.J., Hammarlund, E.U., Haxen, E.R., Su, J., Wang, Y., Canfield, D.E., 2017. Oxygen, climate and the chemical evolution of a 1400 million year old tropical marine setting. Am. J. Sci. 317, 861–900.
Yang, S., Kendall, B., Lu, X., Zhang, F., Zheng, W., 2017. Uranium isotope compositions of mid-Proterozoic black shales: evidence for an episode of increased ocean oxygenation at 1.36 Ga and evaluation of the effect of post-depositional hydrothermal fluid flow. Precambr. Res. 298, 187–201.
Zhang, K., Zhu, X., Wood, R.A., Shi, Y., Gao, Z., Poulton, S.W., 2018. Oxygenation of the Mesoproterozoic ocean and the evolution of complex eukaryotes. Nat. Geosci. 11, 345–350.
Zhang, S., Wang, X., Wang, H., Bjerrum, C.J., Hammarlund, E.U., Costa, M.M., Connelly, J.N., Zhang, B., Su, J., Canfield, D.E., 2016a. Sufficient oxygen for animal respiration 1,400 million years ago. Proc. Natl. Acad. Sci. 113, 1731–1736.
Zhang, S., Wang, X., Wang, H., Bjerrum, C.J., Hammarlund, E.U., Dahl, T.W., Canfield, D.E., 2016b. Reply to Planavsky et al.: Strong evidence for high atmospheric oxygen levels 1,400 million years ago. Proc. Natl. Acad. Sci. 113, E2552-E2553.
Zhang, S., Wang, X., Wang, H., Bjerrum, C.J., Hammarlund, E.U., Haxen, E.R., Wen, H., Ye, Y., Canfield, D.E., 2019. Paleoenvironmental proxies and what the Xiamaling Formation tells us about the mid-Proterozoic ocean. Geobiology 17, 225–246.
Zhang, S., Wang, X., Wang, H., Hammarlund, E.U., Su, J., Wang, Y., Canfield, D.E., 2017. The oxic degradation of sedimentary organic matter 1400Ma constrains atmospheric

oxygen levels. Biogeosciences 14, 2133–2149.
Zhao, G., Cawood, P.A., Wilde, S.A., Sun, M., 2002. Review of global 2.1-1.8 Ga orogens: implications for a pre-Rodinia supercontinent. Earth Sci. Rev. 59, 125–162.
Zhao, Z., 1988. A sedimentary model of the tidal flat of epicontinental sea. Acta Sedimentol. Sin. 6, 68–77 (in Chinese).
Zheng, W., Gilleaudeaua, G.J., Kah, L.C., Anbar, A.D., 2018. Mercury isotope signatures record photic zone euxinia in the Mesoproterozoic ocean. Proc. Natl. Acad. Sci. 115, 10594–10599.
Zheng, Y., Anderson, R.F., van Geen, A., Kuwabara, J., 2000. Authigenic molybdenum formation in marine sediments: a link to pore water sulfide in the Santa Barbara Basin. Geochim. Cosmochim. Acta 64, 4165–4178.